cAMP Activation of Apical Membrane Cl^- Channels: Theoretical Considerations for Impedance Analysis

Teodor G. Păunescu and Sandy I. Helman
Department of Molecular and Integrative Physiology, University of Illinois at Urbana-Champaign, Urbana, Illinois 61801 USA

ABSTRACT Transepithelial electrical impedance analysis provides a sensitive method to evaluate the conductances and capacitances of apical and basolateral plasma membranes of epithelial cells. Impedance analysis is complicated, due not only to the anatomical arrangement of the cells and their paracellular shunt pathways, but also in particular to the existence of audio frequency-dependent capacitances or dispersions. In this paper we explore implications and consequences of anatomically related Maxwell-Wagner and Cole-Cole dielectric dispersions that impose limitations, approximations, and pitfalls of impedance analysis when tissues are studied under widely ranging spontaneous rates of transport, and in particular when apical membrane sodium and chloride channels are activated by adenosine 3′,5′-cyclic monophosphate (cAMP) in A6 epithelia. We develop the thesis that capacitive relaxation processes of any origin lead not only to dependence on frequency of the impedance locus, but also to the appearance of depressed semicircles in Nyquist transepithelial impedance plots, regardless of the tightness or leakiness of the paracellular shunt pathways. Frequency dependence of capacitance precludes analysis of data in traditional ways, where capacitance is assumed constant, and is especially important when apical and/or basolateral membranes exhibit one or more dielectric dispersions.

INTRODUCTION

A variety of hormones including aldosterone and insulin selectively stimulate Na^+ transport in cell-cultured A6 epithelia by increase of the density of functional amiloride-sensitive epithelial Na^+ channels (ENaCs) at the apical membranes of the cells (Blazer-Yost et al., 1996; Baxendale-Cox et al., 1997; Helman et al., 1998). In contrast, hormonal activation of Na^+ transport mediated by the second messenger adenosine 3′,5′-cyclic monophosphate (cAMP) is accompanied by stimulation of Cl^- transport (Yanase and Handler, 1986; Chalfant et al., 1993) involving activation of apical membrane Cl^- channels (Marunaka and Eaton, 1990; Nakahari and Marunaka, 1995; Kokko et al., 1997; Matsumoto et al., 1997). During the course of our studies aimed at understanding the interrelationships among hormones in regulation of Na^+ transport it became necessary to know not only the magnitude of change of the apical membrane cAMP-activated chloride conductance, but also the consequences of activation of the chloride conductance in electrophysiological studies of Na^+ transport, specifically in the A6 epithelium and more generally in other tissues where cAMP activates Na^+ and Cl^- channels.

To address such questions we turned to impedance analysis of the A6 epithelium and found, as in frog skin (Awayda et al., 1999) that the analysis of A6 epithelia was more complicated due principally to audio frequency dielectric relaxation processes or dispersions (Liu and Helman, 1998). In this paper we have used data derived from our studies of A6 epithelia (Păunescu and Helman, 2001) to discuss and illustrate the guiding principles used in experimental design, methods of analysis, and interpretation of data. Although the emphasis of our original inquiry was to understand the role of cAMP in regulation of apical membrane Na^+ and Cl^- channels using methods of impedance analysis, the scope of this project required a rigorous examination of the underlying theoretical considerations and principles that have not appeared in the epithelial transport literature. In this manuscript we emphasize the relevant considerations and principles appropriate to epithelia. The experimental findings presented in a companion paper (Păunescu and Helman, 2001) underscore the need for our theoretical considerations in understanding the mechanisms of hormonal action that activate not only Na^+, but also apical membrane Cl^- channels in A6 epithelia.

Recognition of the existence of plasma membrane frequency-dependent capacitances is critical in the design and interpretation of studies of epithelial tissues. It is of fundamental interest to know the factors and mechanisms underlying audio frequency dielectric dispersions or relaxation processes in epithelial and nonepithelial plasma membranes in terms of the organization of the lipids and proteins of plasma membranes and their structural/functional relationships that give rise to dielectric dispersions at any frequency, and in particular those at audio frequencies (α dispersions (Schwan, 1957)) where transepithelial impedance is usually measured. To the extent that plasma membranes exhibit Cole-Cole-like dielectric dispersions (Cole and Cole, 1941) and to the extent additionally that apical and basolateral membranes form a series arrangement of leaky dielectrics leading to Maxwell-Wagner dispersions, interpretation of changes of capacitance is more complex, requiring consideration not

Received for publication 19 September 2000 and in final form 17 April 2001.

Address reprint requests to Dr. Sandy I. Helman, Dept. of Molecular and Integrative Physiology, University of Illinois at Urbana-Champaign, 524 Burrill Hall, 407 S. Goodwin Ave., Urbana, IL 61801. Tel.: 217-333-7913; Fax: 217-333-1133; E-mail: s-helman@uiuc.edu.

0006-3495/01/08/838/14 $2.00

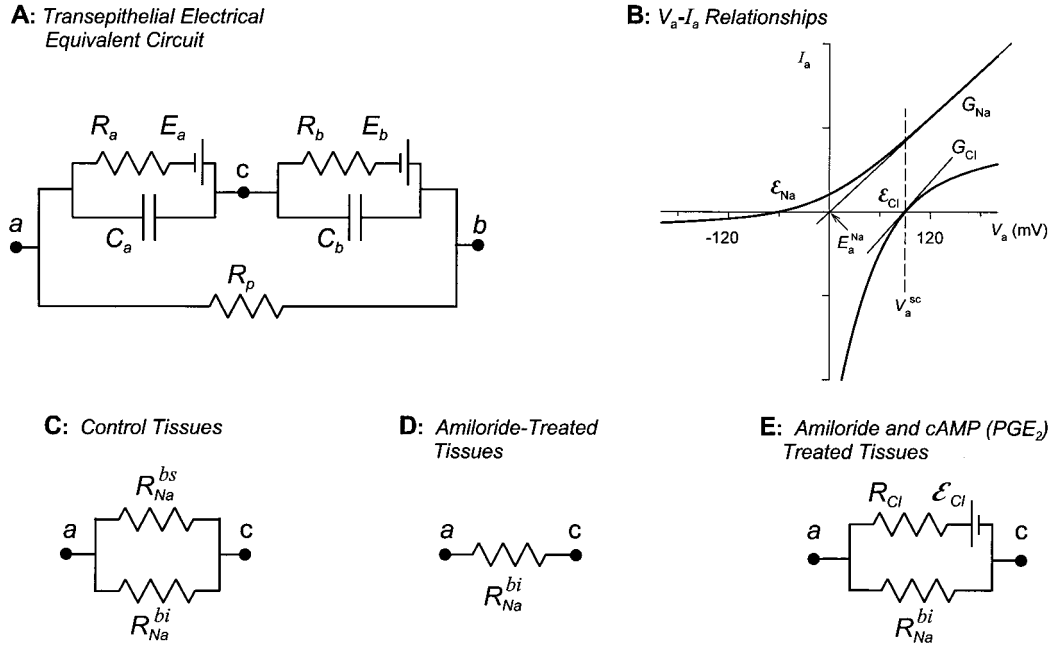

FIGURE 1 (*A*) Transepithelial lumped parameter electrical equivalent circuit of apical and basolateral plasma membranes of the cells shunted by a paracellular resistance, R_p. *a*, *b*, and *c* indicate nodes within the apical, basolateral, and intracellular solutions, respectively. E_a and E_b are Thévenin emfs of apical and basolateral membranes, respectively, with their associated slope resistances, R_a and R_b, and respective capacitances, C_a and C_b. (*B*) Because impedance is measured in the time domain, the conductances must be slope conductances at the operating point voltages of the membranes. Shown are Goldman V_a-I_a relationships (Goldman, 1943) for apical membrane Na^+ and Cl^- channels at the operating point (V_a^{sc}) of short-circuited epithelia that pertain to the conditions of our experiments. Nernst equilibrium potential differences for Na^+ ($\mathcal{E}_{Na}$) and Cl^- ($\mathcal{E}_{Cl}$) are indicated at the points of current reversal. The drawing indicates that whereas Cl^- is at or very near electrochemical equilibrium, Na^+ transport is finite at an apical membrane voltage (V_a^{sc}) far removed from equilibrium in short-circuited tissues ($V_a^{sc} - \mathcal{E}_{Na}$) (Păunescu and Helman, 2001). At V_a^{sc}, the slope conductance for Na^+ is $G_{Na} = R_{Na}^{-1}$ and the Thévenin emf for Na^+ (E_a^{Na}) is at or very near zero mV. The Thévenin emf for Cl^-, E_a^{Cl}, $= \mathcal{E}_{Cl}$. The conductive properties of apical membranes of A6 epithelia are shown in (*C*) for control tissues expressing amiloride-sensitive (R_{Na}^{bs}) and -insensitive (R_{Na}^{bi}) Na^+ channels; in (*D*) for 100 μM amiloride-treated tissues with blocker-insensitive Na^+ channels and in (*E*) for amiloride-blocked tissues treated additionally to increase intracellular cAMP, which activates apical membrane Cl^- channels. $\mathcal{E}_{Cl}$ is included in (*E*) to emphasize that the operating point voltage for Cl^- is close to electrochemical equilibrium, whereas the distribution for Na^+ across the apical membrane is far removed from its electrochemical equilibrium with a Thévenin emf, E_{Na}, at or very near zero. From the point of view of impedance, the emfs (Nernst or Thévenin) are irrelevant, but the slope conductances will vary with voltage due to the degree of nonlinearity of the *V-I* relationships at the operating points of membrane voltage.

only of membrane areas and thicknesses but also those factors that can change the frequency-dependent dielectric properties of the membrane and hence, the capacitance measured at any frequency.

THEORETICAL CONSIDERATIONS

Electrical equivalent circuits

In the face of nonlinear current-voltage relationships of the underlying channels and electrodiffusive transporters, impedance analysis requires electrical equivalent circuits where membranes are modeled by their slope resistances ($R = \Delta V/\Delta I$). Hence, as indicated in Fig. 1 *A*, the resistances R_a, R_b, and R_p are the slope resistances of the apical membrane, basolateral membrane, and paracellular shunt, respectively. Because the resistances are slope resistances, the E_a and E_b are the Thévenin emfs of the apical and basolateral membranes, respectively (Chua, 1969; Helman and Thompson, 1982). It is important when dealing with nonlinear circuits to distinguish between chord and slope formalisms of electrical circuit theory. In our notation we have used *R*'s and *G*'s to indicate slope resistances and conductances (as compared to *g*'s in the chord formalism), and used *E*'s for Thévenin emfs that are not necessarily the same as the $\mathcal{E}$'s that designate Nernst equilibrium potential differences. Thus, as indicated in Fig. 1 *A*, the epithelium is modeled as a series arrangement of apical and basolateral membrane impedances that exists in parallel with a paracellular shunt resistance, R_p. The respective slope resistances R_a and R_b and capacitances C_a^* and C_b^* of apical and basolateral membranes give rise to the apical and basolateral membrane impedances Z_a and Z_b, so that the transepithelial impedance Z_T is:

$$Z_T = \frac{(Z_a + Z_b)R_p}{Z_a + Z_b + R_p} \quad (1)$$

and where:

$$Z_a = \frac{R_a}{1 + j\omega R_a C_a^*} \quad (2)$$

$$Z_b = \frac{R_b}{1 + j\omega R_b C_b^*} \quad (3)$$

The notation of asterisk-superscripted C's indicates that capacitance may be complex (frequency-dependent). If the C's are complex, then the time constants, RC^*, are also frequency-dependent. At the limiting frequency bounds, Z_T approaches zero at infinite frequency; as frequency approaches zero, Z_T approaches the transepithelial slope resistance, $R_T = [(R_a + R_b)R_p]/(R_a + R_b + R_p)$. If the capacitances at the audio frequencies of impedance measurements exhibit Maxwell-Wagner and/or Cole-Cole dispersions (Awayda et al., 1999) (or dielectric dispersions from any other source), such dispersions will give rise to power law dependence of the impedance (see below).

Shown also in Fig. 1 are the electrodiffusive or conductive components of R_a in three transport states of the tissues. In their control state (Fig. 1 *C*), A6 epithelia, otherwise untreated by hormones or second messengers that activate Cl^- channels, express both blocker-sensitive (*bs*) and to a much lesser extent blocker-insensitive (*bi*) Na^+ currents that account completely for the total current or the net rates of Na^+ entry into the cells as measured by short-circuit currents (Baxendale-Cox et al., 1997; Helman et al., 1998). As indicated, R_a is partitioned between blocker-sensitive (R_{Na}^{bs}) and blocker-insensitive (R_{Na}^{bi}) slope resistances. Notably, the Thévenin emfs of these Na^+ conductances (E_a^{Na}) are at or very near zero, because as indicated in Fig. 1 *B*, the slope conductance, G_{Na}, at the operating point of the apical membrane voltage (V_a^{sc}) intersects the voltage axis at or very near zero when V_a^{sc} is very far removed from electrochemical equilibrium ($\mathcal{E}_{Na}$) (Helman and Thompson, 1982). Accordingly, the blocker-sensitive and -insensitive Na^+ currents are $I_{Na}^{bs} = V_a/R_{Na}^{bs}$ and $I_{Na}^{bi} = V_a/R_{Na}^{bi}$. With amiloride block of apical membrane ENaCs, the apical membrane R_a reduces to the R_{Na}^{bi}, as indicated in Fig. 1 *D*. With I_{Na}^{bi} averaging much less than 0.5 $\mu A/cm^2$ (Helman and Liu, 1997; Baxendale-Cox et al., 1997; Blazer-Yost et al., 1999; Păunescu et al., 2000) and V_a exceeding 100 mV under these conditions, the R_{Na}^{bi} is expected to be far greater than 200,000 $\Omega \cdot cm^2$.

Activation of apical membrane Cl^- channels introduces a slope conductance $G_{Cl} = 1/R_{Cl}$ with a Thévenin E_{Cl}. If, as indicated in Fig. 1, *B* and *E*, Cl^- is distributed across the apical membrane at or very near the Nernst equilibrium potential difference, $\mathcal{E}_{Cl}$, then E_{Cl} can be replaced by $\mathcal{E}_{Cl}$. To the extent that $R_{Na}^{bi} \gg R_{Cl}$, $R_a \approx R_{Cl}$ at the operating point of the apical membrane voltage, which as indicated elsewhere (Păunescu and Helman, 2001) is very close to $\mathcal{E}_{Cl}$.

For purpose of discussion below we have used values of resistance and capacitance in the range(s) that we believe are relevant to those of A6 epithelia studied in our laboratory (Liu and Helman, 1998; Păunescu et al., 2000; Păunescu and Helman, 2001). In amiloride-blocked states of Na^+ transport, $R_a = R_{Na}^{bi}$ is near 500 $k\Omega \cdot cm^2$ and R_b averages near 4000 $\Omega \cdot cm^2$. R_b may vary with the rate of Na^+ transport (Păunescu et al., 2000) but there is presently insufficient information to know if this is so in A6 epithelia and to what extent. The R_a of control tissues is highly variable and depends on the rate of Na^+ transport (short-circuit currents) where the spontaneous amiloride-sensitive I_{sc} can range downward to values <1 $\mu A/cm^2$ ($R_{Na}^{bs} > 112$ $k\Omega \cdot cm^2$) and upward to >30 $\mu A/cm^2$ ($R_{Na}^{bs} < 3.7$ $k\Omega \cdot cm^2$). The static *dc* or zero-frequency capacitances of apical (C_a^{dc}) and basolateral membranes (C_b^{dc}) average near 1.5 and 20 $\mu F/cm^2$, respectively (Păunescu and Helman, 2001). Thus, for the monolayers of A6 epithelia where basolateral membrane area is considerably less than in the functionally coupled cells of the multicellular layers of frog skin, the basolateral membrane resistance of A6 epithelia is about four times greater and the capacitance about three times less than observed in studies of frog skin (Awayda et al., 1999). Accordingly, and unlike in frog skin, where the impedance of the basolateral membranes under some experimental conditions may approach negligible values, the Z_b of A6 epithelia cannot be neglected at any frequency, as will be indicated below.

Interpretation of transepithelial impedance data and the design of experiments to evaluate the tissues is complicated not only by the juxtaposed impedance of the cells ($Z_a + Z_b$) and their paracellular shunts (R_p), but also by the possibility that the plasma membranes exhibit capacitive dispersions at the frequencies of interest. A simplification of experimental conditions utilizes amiloride to block apical membrane epithelial Na^+ channels (ENaCs) so that at least at very low frequencies, $Z_a \gg Z_b$ and the cellular resistance ($R_{cell} = R_a + R_b$) is much greater than R_p. Accordingly, with $R_a \gg R_b$ and $R_{cell} \gg R_p$, the measured transepithelial resistance, R_T, closely approaches the values of R_p. At very high frequencies, where the R_a and R_b become negligible relative to their respective capacitive reactances, the equivalent capacitance of the cells, C_{eq}^*, approaches values of the series arrangement of capacitance $(C_a^* C_b^*)/(C_a^* + C_b^*)$, where notably such values would not be the same as $(C_a^{dc} C_b^{dc})/(C_a^{dc} + C_b^{dc})$ if either or both apical and basolateral membranes exhibit dielectric dispersions. Thus, we have considered in more detail the behavior of the transepithelial impedance in amiloride-treated tissues first. Also, it will be evident below that it is critically important to know with reasonable certainty the values of R_p especially under conditions where R_a is not much greater than R_b and R_p, as would be the case for tissues transporting Na^+ or for tissues in their amiloride or non-amiloride pretreated state where cAMP activates apical membrane Cl^- channels.

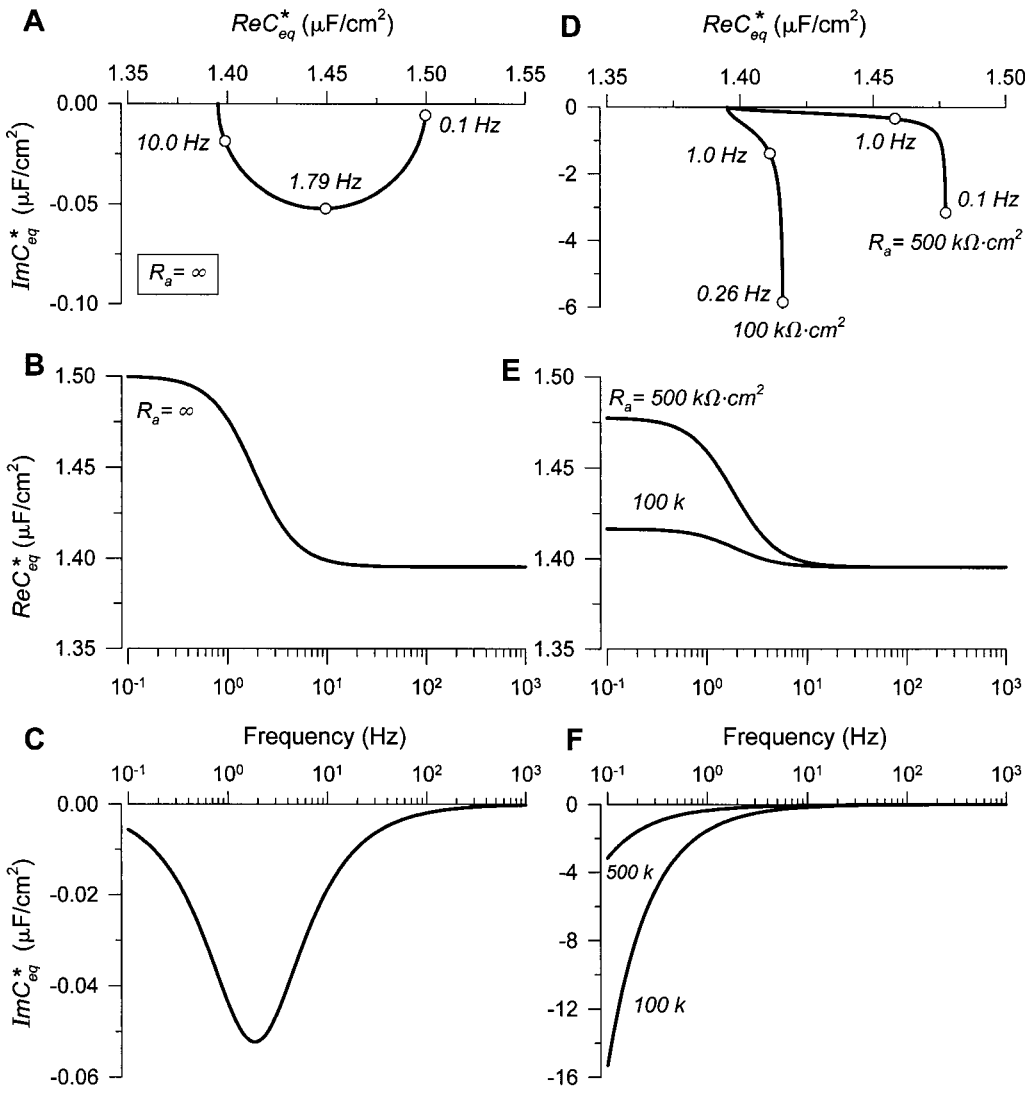

FIGURE 2 Nyquist (*A*) and Bode plots (*B* and *C*) are shown for the equivalent complex capacitance, C^*_{eq}, of a transcellular Maxwell-Wagner dispersion if $R_a = \infty$. Maxwell-Wagner plots of C^*_{eq} are shown in (*D*) (Nyquist) and (*E*) and (*F*) (Bode) when R_a = 100 kΩ · cm² and 500 kΩ · cm². R_b = 4000 Ω · cm², C_a = 1.5 μF/cm², C_b = 20.0 μF/cm². The capacitances are assumed to be independent of frequency.

FREQUENCY-DEPENDENT CAPACITANCE

Maxwell-Wagner dispersions

Although the measurement of impedance is straightforward, the analysis and interpretation of data is complicated when capacitances are frequency-dependent. Frequency-dependent capacitances may arise from Maxwell-Wagner dispersions (Daniel, 1967; Jonscher, 1983) due to the juxtaposition of leaky dielectrics that exist in series. From the transepithelial point of view, the apical and basolateral membranes of the cells behave as a series arrangement of leaky dielectrics with capacitances C_a and C_b paralleled by resistances R_a and R_b, respectively, as indicated in Fig. 1 *A*. Accordingly, the transcellular impedance behaves as a complex frequency-dependent equivalent capacitance, C^*_{eq}, where:

$$C^*_{eq} = [j\omega(Z_a + Z_b)]^{-1} \quad (4)$$

Nyquist and Bode plots of C^*_{eq} are plotted in Fig. 2. For the case where R_a is infinite and where C^{dc}_a = 1.5 μF/cm², C^{dc}_b = 20 μF/cm², and R_b = 4000 Ω · cm², C^*_{eq} decreases from the C^{dc}_a of 1.5 μF/cm² to 1.395 μF/cm² as frequency increases toward ~100–200 Hz. Despite the fact that C_a and C_b are constant at all frequencies, the series arrangement of membranes gives rise to a Maxwell-Wagner dispersion at low audio frequencies so that the cells behave as a frequency-dependent capacitance that exists in parallel with the R_p. The dispersion appears as an ideal semicircle in Nyquist

plots with a characteristic frequency at the apex of the semicircle of 1.79 Hz, as indicated in Fig. 2 *A*. When R_a is not infinite and in the range of 100–500 k$\Omega \cdot cm^2$ as illustrated in Fig. 2 *D*, the C^*_{eq} due to Maxwell-Wagner dispersions are quantitatively more complex, reflecting the fact that a finite value of resistance behaves in the equivalent sense as a frequency-dependent capacitance ($C(\omega) = (j\omega R)^{-1}$). Accordingly, as illustrated in Fig. 2, *D–F*, the imaginary components of C^*_{eq} (ImC^*_{eq}) become enormous in value relative to those of the real components of C^*_{eq} (ReC^*_{eq}) as frequency decreases toward zero. Thus, despite relatively high values of R^{bi}_a in amiloride-blocked tissues, such values of R_a will markedly affect the magnitudes and phases of the C^*_{eq} at low frequencies $<\sim$100 Hz for the parameters of the circuit used here in our calculations (Fig. 2, *E* and *F*). If capacitances do not exhibit dielectric dispersions at higher frequencies than ~100 Hz, then with C_a = 1.5 μF/cm^2 and C_b = 20 μF/cm^2, C_{eq} would be 1.395 μF/cm^2 at higher frequencies beyond those expected of the Maxwell-Wagner dispersions. Indeed, because C_b is considerably larger than C_a, the Maxwell-Wagner frequency-dependent decrement of C^*_{eq} is relatively small (7%), but nevertheless important at the lower audio frequencies where attempts are made to determine the *dc* capacitances. Such considerations are especially important in those tissues that spontaneously transport Na^+ at low rates, in tissues where Na^+ transport is suppressed by drugs, hormones, or other experimental maneuvers that affect R^{bs}_{Na}, and in particular in those tissues treated with amiloride to completely inhibit blocker-sensitive apical membrane Na^+ channels. With shunt resistances in the range of 10 k$\Omega \cdot cm^2$, the useful frequency range of interest (see below) includes those frequencies down to ~0.1 Hz, where Maxwell-Wagner dispersions will affect the magnitudes and phases of the transepithelial impedance. It must be stressed, owing to the series arrangement of apical and basolateral membranes of epithelia in general, that Maxwell-Wagner dispersions are unavoidable regardless of the magnitudes of conductances and capacitances in tight and leaky epithelia and regardless of additional dispersions that may arise from the plasma membrane dielectrics.

Thus, independent of the values of R_a, interpretation of measurements of impedance can be problematic at very low frequencies due to unavoidable Maxwell-Wagner dispersions.

Cole-Cole dielectric dispersions

In contrast to Maxwell-Wagner dispersions, frequency-dependent capacitances can also arise from dielectric relaxation processes as described originally by Cole and Cole, Schwan, and others (Cole and Cole, 1941; Schwan, 1957; Kell and Harris, 1985; Takashima, 1989) and can be associated with C_a and/or C_b. When observed at audio frequencies these relaxation processes are refereed to as α dispersions, while those at higher radio frequencies have been referred to as β dispersions. Our considerations in this paper will be limited to α dispersions. Plasma membranes may exhibit multiple relaxation processes (Eq. 5) (Cole and Cole, 1941; Awayda et al., 1999) where the complex capacitance C^* at any frequency will vary with the magnitudes of the dielectric increments (C_i), the time constants (τ^r_i), or characteristic frequencies (f^r_i) of the relaxation processes and power law coefficients (α_i) that lead to observation of depressed semicircles in Nyquist plots of C^*. C^∞_α represents the limiting static capacitance at frequencies far greater than the highest relaxation frequency process ($f^r_i = (2\pi\tau^r_i)^{-1}$) that exists in the audio range of frequencies.

Resolving plasma membrane dielectric relaxation processes in intact epithelial tissues at high frequencies is limited by the uncertainties in measurement of the exact magnitude of the series solution resistance of the cell cytoplasm and the solutions bathing the apical and basolateral borders of the tissues. With high values of capacitance (1.5 μF/cm^2), the capacitive reactance of C_a at 10 kHz is 10.6 $\Omega \cdot cm^2$ and only 1.06 $\Omega \cdot cm^2$ at 100 kHz, which approaches the value of the cytoplasmic resistance of the cells. Thus, detection of dispersions that exist in the range of radio frequencies (β dispersions) or higher frequencies is essentially if not completely precluded because the errors in determining Z_T from small differences between the measured impedances and those of the series resistances of the cells and bathing solutions cannot be adequately assessed. Thus, our experiments and our considerations are limited to audio frequency α dispersions of the type described by Eq. 5.

$$C^* = \sum_{i=1}^{n} \frac{C_i}{1 + (j\omega\tau^r_i)^{\alpha_i}} + C^\infty_\alpha \qquad (5)$$

Illustrated in Fig. 3, *A–C* are Nyquist and Bode plots of a single relaxation process. We have assumed, based upon our experimental findings (Păunescu and Helman, 2001) that the apical membrane is characterized by a Cole-Cole relaxation process, so that the complex apical membrane capacitance, C^*_a, can be calculated with Eq. 5. The *dc* capacitance, C^{dc}_a, is 1.5 μF/cm^2 (Păunescu and Helman, 2001). The dielectric increment, $C_{1a} = C^{dc}_a - C^\infty_a$, is 0.6 μF/cm^2 with a relaxation frequency of 110 Hz. The complex capacitance approaches C^∞_a = 0.9 μF/cm^2 as frequency far exceeds 10 kHz approaching values near 1 MHz. The semicircle is depressed due to a power law dependence of the capacitance, α_a = 0.6, which is consistent with the idea that there is a distribution of time constants (Cole and Cole, 1941; Cole, 1968; Gabler, 1978; Pethig, 1979; Jonscher, 1983) of the relaxation processes centered at a relaxation frequency of 110 Hz. For such dispersions the complex capacitance vectors vary in magnitude ($|C^*_a|$) and phase angle (ϕ) as indicated in the Nyquist plots (Fig. 3 *A*) or in rectangular

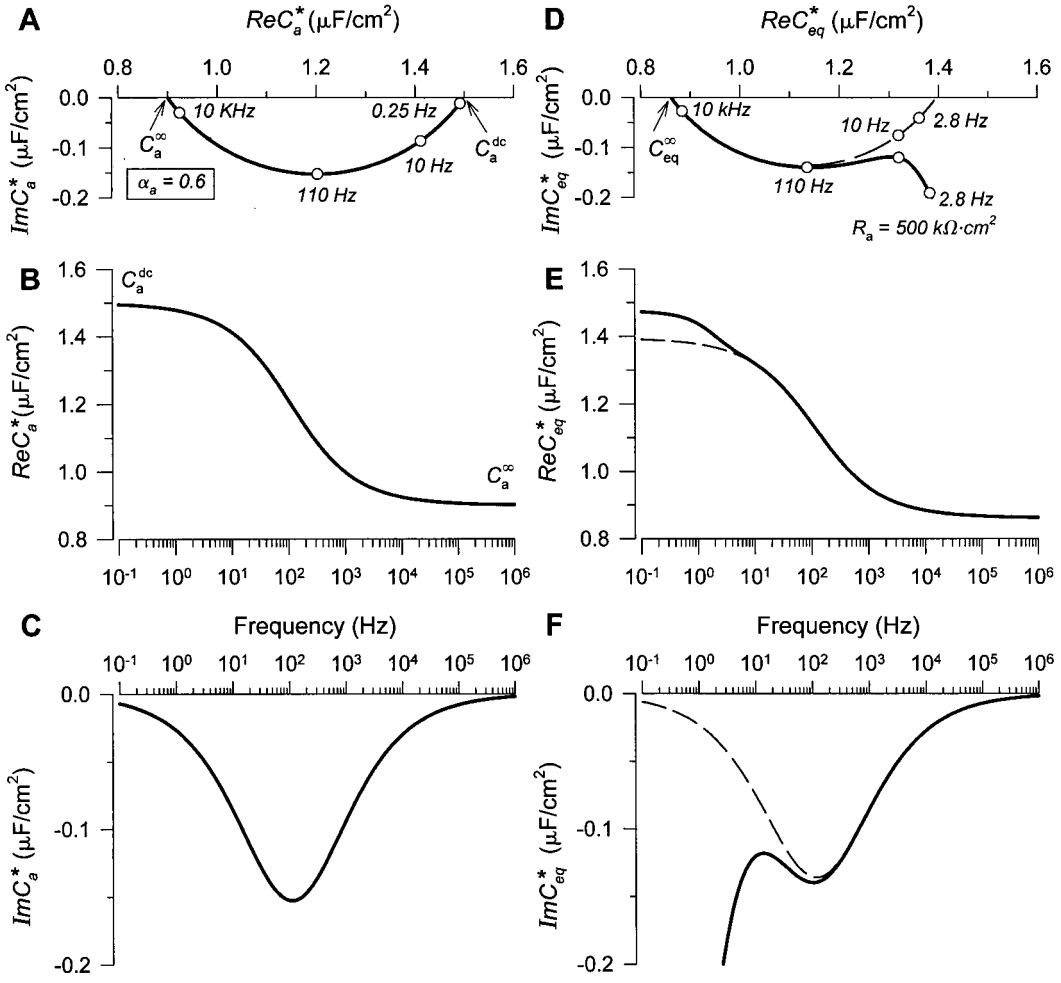

FIGURE 3 Apical membrane Nyquist (*A*) and Bode plots (*B* and *C*) are shown for the complex capacitance C_a^* of a Cole-Cole audio frequency α dispersion with a relaxation frequency of 110 Hz and power law dependence, $\alpha_a = 0.6$. The transcellular complex equivalent capacitance, C_{eq}^*, is shown in Nyquist (*D*) and Bode plots (*E* and *F*) when the apical membrane capacitance exhibits an α dispersion as in (*A*). $R_a = 500\ k\Omega \cdot cm^2$; $R_b = 4000\ \Omega \cdot cm^2$, and $C_b = 20.0\ \mu F/cm^2$. The dashed lines in (*D*)–(*F*) indicate the C_{eq}^* if $R_a = R_b = \infty$.

coordinates as the real (ReC_a^*) and imaginary (ImC_a^*) components of C_{eq}^* as indicated in Fig. 3, *B* and *C*, respectively. The absolute magnitude of ImC_a^* is maximal at the relaxation frequency of 110 Hz (Fig. 3 *C*). The ReC_a^* is decreased from C_a^{dc} by one-half of the magnitude of the dielectric increment ($C_{1a} = C_a^{dc} - C_a^\infty$) at 110 Hz (Fig. 3 *B*). It should be noted that $\alpha_a = -2ImC_a^*/C_{1a}$ where $0 \leq \alpha_a \leq 1$.

Combined Maxwell-Wagner and Cole-Cole dispersions

With Maxwell-Wagner dispersions dominant at lower frequencies and α dispersions at higher frequencies, resolving the α dispersions at lower frequencies is complicated, as illustrated in Fig. 3, *D–F*. Regardless of the values of R_a and assuming for the sake of simplicity that C_b is devoid of α dispersions, the behavior of C_{eq}^* at frequencies $<\sim$100–200 Hz is markedly influenced by the Maxwell-Wagner dispersion. If, additionally, C_b exhibits α dispersions, the behavior of C_{eq}^* would be more complex especially at the lower frequencies. Consequently, from the transepithelial point of view, capacitance of the cells would appear frequency-dependent over the entire range of audio frequencies, where at higher frequencies the changes of capacitance would be dominated by the α dispersions but with more complex behavior at the lower frequencies due to the Maxwell-Wagner dispersion. Assuming, as indicated above, that C_b (20 $\mu F/cm^2$) is devoid of α dispersions, the C_{eq}^∞ is 0.861 $\mu F/cm^2$ (Fig. 3, *D* and *E*) and the C_{eq}^{dc} would be 1.395 $\mu F/cm^2$ if R_a and R_b were infinitely large, as indicated by the dashed lines in these figures. The contribution of the Maxwell-Wagner dispersion to C_{eq}^* can be assessed by examination of the differences of C_{eq}^* when R_a and R_b are either finite or infinite in value.

Determination of the complex equivalent capacitance, C^*_{eq}

C^*_{eq} is best determined under conditions where ideally R_a is infinitely high so that the transepithelial resistance is due solely to the shunt resistance, R_p. Under such conditions the transepithelial impedance is determined by the parallel combination of R_p and C^*_{eq} so that:

$$Z_T = \frac{R_p}{1 + j\omega R_p C^*_{eq}} \quad (6)$$

Rearranging Eq. 6 allows calculation of the C^*_{eq} from the measured values of Z_T. [It should be noted according to Eq. 6 and the definition of the complex capacitance, C^*_{eq}, in Eq. 4 that the transepithelial impedance of an epithelium can always be modeled by an R_p paralleled by the cellular impedance ($Z_a + Z_b$) regardless of the tightness or leakiness of the junctional complexes in the paracellular shunt pathways of the epithelium. To the extent that R_a is practically infinitely large, as in amiloride-blocked tissues with unstimulated intracellular levels of cAMP, R_p can be equated directly with the R_T and determined from the measured values of Z_T as frequency approaches zero, thereby simplifying analysis, as R_p can be measured directly. When R_a cannot be neglected, R_p must be determined by an independent method because $R_p > R_T$.] To the extent that R_a can vary over wide ranges depending on the rates of Na^+ transport, it is always possible to use amiloride to block Na^+ channels ($R^{bs}_{Na} \rightarrow \infty$) thereby elevating R_a to values of R^{bi}_{Na} that will exceed 200 k$\Omega \cdot cm^2$ (see above) when the amiloride-insensitive Na^+ currents are <0.5 $\mu A/cm^2$. Under these amiloride-blocked conditions where $R_a \gg R_b$, the transepithelial resistance, R_T, approaches values of the parallel combination of R_a and R_p or values of R_p when $R_a \gg R_p$. Thus, with R_p averaging near 10 k$\Omega \cdot cm^2$ and cell resistances much greater than 200 k$\Omega \cdot cm^2$, C^*_{eq} determined with Eq. 6 would to a very good approximation provide data that would allow discrimination between dispersions arising from Maxwell-Wagner behavior and dielectric relaxation processes. Plotted in Fig. 4 are the magnitudes, $|C^*_{eq}|$, and phase angles, ϕ, of C^*_{eq} for R_a between 100 k$\Omega \cdot cm^2$ and infinity attributable alone to the Maxwell-Wagner dispersion. At frequencies $>\sim$10 Hz, $|C^*_{eq}|$ is constant. However, at frequencies $<$10 Hz, $|C^*_{eq}|$ increases precipitously as frequency decreases at finite values of R_a. Accordingly, despite block of the amiloride-sensitive Na^+ channels, the Maxwell-Wagner effect makes it appear as though capacitance exceeds the actual C^{dc}_a of 1.5 $\mu F/cm^2$. This is a pitfall of the analysis where what seemingly may be a reasonable assumption, namely a very high and "negligible" value of R_a relative to R_b and R_p, is in fact a poor assumption when analysis of data is carried out at low frequencies (see below) in the range of the Maxwell-Wagner dispersions. Not only are the $|C^*_{eq}|$ overestimated at frequencies $<$10 Hz, the phase angles of C^*_{eq} also vary with frequency up to 1 MHz when

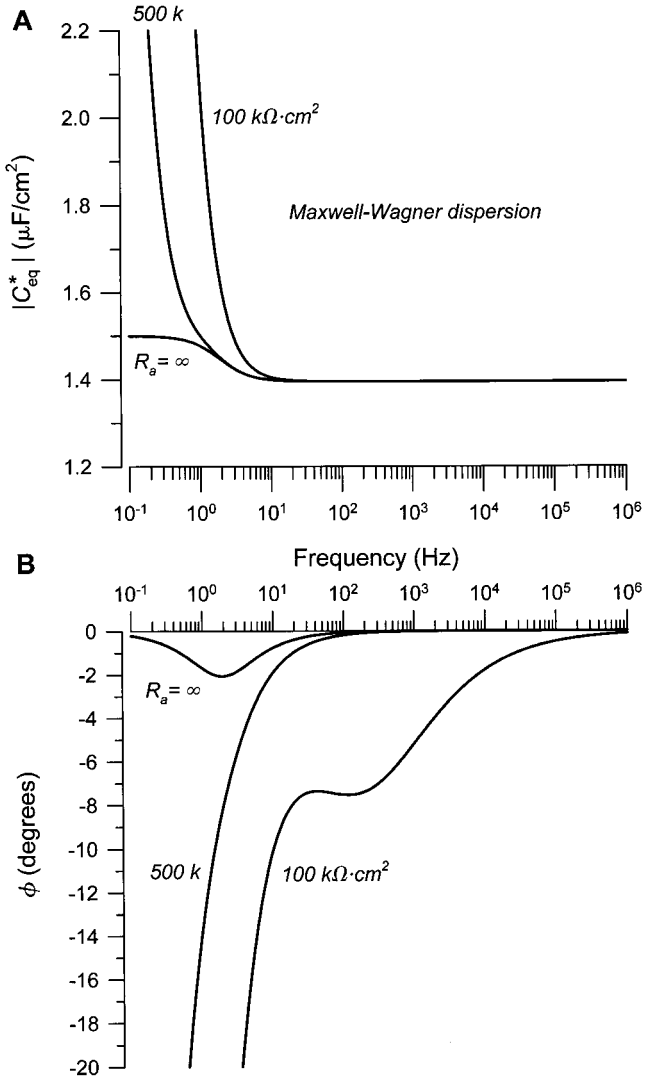

FIGURE 4 Shown are the frequency-dependent absolute magnitudes ($|C^*_{eq}|$) (*A*) and phase angles in degrees (ϕ) (*B*) of a transcellular Maxwell-Wagner dispersion when $R_a = \infty$, 100 k$\Omega \cdot cm^2$, or 500 k$\Omega \cdot cm^2$. R_b = 4000 $\Omega \cdot cm^2$, C_a = 1.5 $\mu F/cm^2$, C_b = 20.0 $\mu F/cm^2$. Note that the values of $|C^*_{eq}|$ can exceed C_a (1.5 $\mu F/cm^2$) as frequency decreases (see text).

R_a is 100 k$\Omega \cdot cm^2$ (Fig. 4 *B*). It is important to realize that with R_p's in the range of 10 k$\Omega \cdot cm^2$ the characteristic frequencies of impedance ($f^z = (2\pi R_p|C^*_{eq}|)^{-1}$) are in the range of 10 Hz, so that impedance measured at these lower frequencies is especially sensitive to changes of capacitance associated with Maxwell-Wagner dispersions.

Although the Maxwell-Wagner effect on $|C^*_{eq}|$ is dominant at low frequencies, the dielectric dispersions are readily distinguished from those of Maxwell-Wagner at higher frequencies, as indicated in Fig. 5 *A*. For the relaxation process centered at 110 Hz, which we have used in our considerations of A6 epithelia, the $|C^*_{eq}|$ are virtually the same at frequencies $>\sim$30–40 Hz irrespective of the values of $R_a \geq 100$ k$\Omega \cdot cm^2$. An analysis such as this can and should

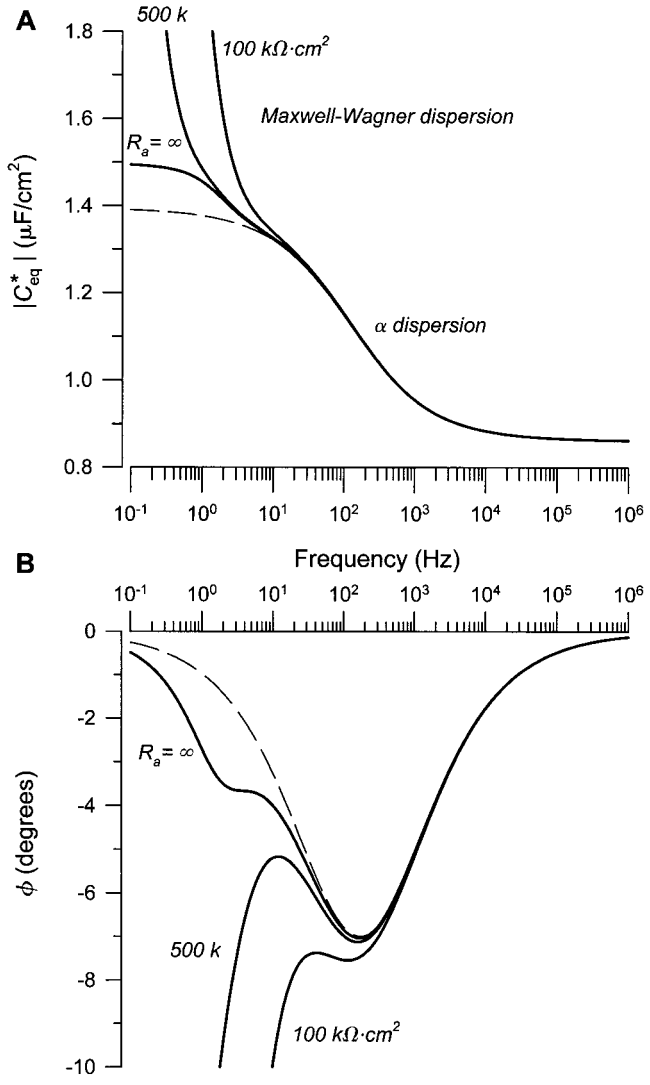

FIGURE 5 Shown are the frequency-dependent absolute magnitudes ($|C^*_{eq}|$) (*A*) and phase angles in degrees (ϕ) (*B*) of a transcellular Maxwell-Wagner dispersion where the apical membrane capacitance, C^*_a, is complex ($C^{dc}_a = 1.5\ \mu F/cm^2$, $C^{\infty}_a = 0.9\ \mu F/cm^2$, $f^{\tau} = 110$ Hz, $\alpha_a = 0.6$). $R_a = \infty$, 100 k$\Omega \cdot cm^2$, or 500 k$\Omega \cdot cm^2$. $R_b = 4000\ \Omega \cdot cm^2$, $C_b = 20.0\ \mu F/cm^2$.

be done for any set of parameters. Our calculations presented here apply only to those values that we have reason to believe are representative of A6 epithelia studied in our own laboratory.

We emphasize that our analysis for the purpose of discussion presumes that an α dielectric dispersion occurs only at the apical membranes of the cell. Quite generally, there may be more than one α dispersion at apical membranes and it is likely that basolateral membranes also exhibit α dispersions. Presently, we have no specific information on the dielectric behavior of any basolateral membrane. It is nevertheless clear that with values of C^{dc}_b much greater than those of C^{dc}_a (20 vs. 1.5 $\mu F/cm^2$), the contribution of basolateral membrane dielectric dispersions to the values of C^*_{eq} would be relatively small compared to those arising from the apical membrane if the dispersions at both membranes are proportionally the same. Thus, it is more likely that if α dispersions are observed under the conditions considered here, they arise from the apical membranes of the cells (however, see also below).

It should be recognized that A6 epithelia are capable of wide ranging rates of spontaneous Na^+ transport with lower limits near 1 $\mu A/cm^2$. In such tissues the values of R_a will be near 100 k$\Omega \cdot cm^2$. Consequently, from the point of view of transepithelial impedance, such low transport rate tissues will behave more like amiloride-blocked tissues. However, when apical membrane conductance to Na^+ is spontaneously high or when Cl^- conductance is activated by cAMP in the presence or absence of amiloride, it would no longer be possible to assume, as above, that values of R_T approach values of R_p. R_a may also be either larger or smaller than R_b. Such conditions impose special limitations in evaluation of the frequency-dependent characteristics of the plasma membranes (see below). Consequently, our discussion to follow focuses on experimental conditions where $R_a \gg R_p$, and in particular on the influence of the R_p on the analysis of experimental data.

IMPEDANCE

Depressed impedance loci (semicircles) in Nyquist plots ($R_a \gg R_b$)

It has been a consistent and inviolate observation in our laboratory (Liu and Helman, 1998; Awayda et al., 1999; Păunescu and Helman, 2001) and others (Schifferdecker and Fromter, 1978; Gordon et al., 1989) that Nyquist impedance plots invariably exhibit depressed semicircular behavior regardless of the state of transport of the epithelium studied ($R_a > R_b$; $R_a < R_b$), requiring fitting equations with power law dependence to account for the depressed locus of the impedance vectors. Complex frequency-dependent capacitances give rise to power law dependencies of impedance as indicated below. Eq. 6 can be rewritten as:

$$Z_T = \frac{R_p}{1 + j\omega R_p(\mathrm{Re}C^*_{eq} - j \cdot \mathrm{Im}C^*_{eq})} \tag{7}$$

which can be expanded in rectangular coordinates ($\mathrm{Re}Z_T - j \cdot \mathrm{Im}Z_T$) to:

$$Z_T = \frac{1 + (\omega R_p \mathrm{Im}C^*_{eq})}{(1 + \omega R_p \mathrm{Im}C^*_{eq})^2 + (\omega R_p \mathrm{Re}C^*_{eq})^2} - j\frac{(\omega R_p^2 \mathrm{Re}C^*_{eq})}{(1 + \omega R_p \mathrm{Im}C^*_{eq})^2 + (\omega R_p \mathrm{Re}C^*_{eq})^2} \tag{8}$$

At the frequency $\omega = 2\pi f^z = (R_p|C^*_{eq}|)^{-1}$:

$$f^z = \frac{1}{2\pi R_p \sqrt{\mathrm{Re}C^{*2}_{eq} + \mathrm{Im}C^{*2}_{eq}}} \quad (9)$$

and it is readily shown that the $\mathrm{Re}Z_T = R_p/2$ when $f = f^z$, regardless of the value of the $\mathrm{Im}Z_T$ (or regardless of the degree of depression of the impedance locus). Defining the degree of depression of the Nyquist impedance semicircle, γ, as $\mathrm{Im}Z_T/\mathrm{Re}Z_T = 2 \cdot \mathrm{Im}Z_T/R_p$ at $f = f^z$, γ is:

$$\gamma = \left.\frac{\mathrm{Re}C^*_{eq}}{\sqrt{\mathrm{Re}C^{*2}_{eq} + \mathrm{Im}C^{*2}_{eq}} + \mathrm{Im}C^*_{eq}}\right|_{f=f^z} \quad (10)$$

Consequently, depression of the impedance semicircles in Nyquist plots is independent of the magnitude of R_p. It should be noted and emphasized that depression of the impedance locus requires $|\mathrm{Im}C^*_{eq}| > 0$, like those that arise with Maxwell-Wagner and Cole-Cole α dispersions. It should be appreciated that if $\mathrm{Im}C^*_{eq}$ is zero, then change alone of $\mathrm{Re}C^*_{eq}$ does not give rise to a depressed impedance locus.

To illustrate the relative importance of the $\mathrm{Im}C^*_{eq}$ and $\mathrm{Re}C^*_{eq}$ on depression of the impedance locus we calculated γ for a simple parallel combination of an R_p and an apical membrane with a single Cole-Cole relaxation process where C^{dc}_a was 1.5 μF/cm^2 and where C^{∞}_a was 0.5, 0.9, or 1.2 μF/cm^2, thereby giving dielectric increments of 1.0, 0.6, and 0.3 μF/cm^2, respectively, at characteristic frequencies of 110 Hz, as above. Depression of capacitance, α_a, was varied between extremes of 0 and 1.

The relationship between α_a and γ is nonlinear and inverse as illustrated in Fig. 6. The degree of depression of the impedance locus will vary not only with the magnitude of the dielectric increment but also requires, as indicated above, that $\alpha_a > 0$ (or $\mathrm{Im}C^*_{eq} \neq 0$). It is also apparent that the maximal influence of the capacitive dispersion occurs when α_a approaches unity. Although we have dealt here with specific values to illustrate a point, this discussion can be generalized to any frequency-dependent dielectric behavior (and to Maxwell-Wagner behavior) which, according to the generalized thesis presented above (Eqs. 7–10), may be used to argue for the existence of frequency-dependent capacitances when the impedance locus is depressed.

Depressed Nyquist impedance loci are plotted in Fig. 7 *A* for epithelia with apical and basolateral membrane characteristics described above. The α_a are 0.25, 0.5, 0.75, and 1.0 and R_p = 1000 $\Omega \cdot$ cm^2 (C^{dc}_a = 1.5 μF/cm^2; C^{∞}_a = 0.9 μF/cm^2; f^r = 110 Hz; R_a = 500 k$\Omega \cdot$ cm^2; R_b = 4000 $\Omega \cdot$ cm^2; C_b = 20 μF/cm^2). Depression of $\mathrm{Im}Z_T$ is maximal at α_a = 1.0 (Fig. 7, *A* and *C*) at frequencies near 142 Hz for α_a = 0.25, 0.50, and 0.75 and near 148 Hz for α_a = 1.0 (Fig. 7 *C*). The corresponding values of γ and α_a are given in Fig. 7 *C*; γ ranges between 0.785 and 0.953 for α_a between 1.0 and 0.25. Although the maximal absolute values of $\mathrm{Im}Z_T$ exist at frequencies very close to those expected when $\mathrm{Re}Z_T = R_p/2$, the small deviations from ideal depressed semicircles exist because of the greater contribution of the Maxwell-Wagner dispersion to the impedance at the lower frequencies leading to an asymmetry in the impedance locus.

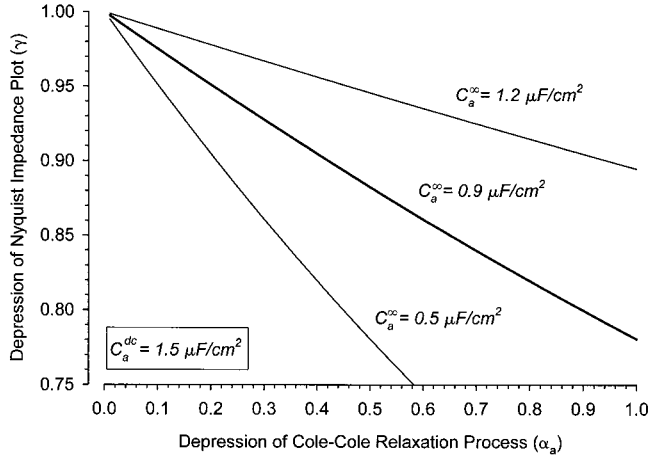

FIGURE 6 Relationship between power law dependence of Cole-Cole dispersion (α_a) (depression of complex capacitance) and depression of impedance semicircles in Nyquist plots (γ) (see text).

The exact impedance locus will depend not only on the capacitive dispersions but also on the values of R_p, because R_p is a major component of transepithelial impedance that will determine the frequencies at $\mathrm{Re}Z_T = R_p/2$. For R_p's of 1, 10, and 50 k$\Omega \cdot$ cm^2 (Fig. 8, *A–C*), the corresponding frequencies are 142.2, 12.09, and 2.45 Hz. Thus, in tissues with very high R_p = 50 k$\Omega \cdot$ cm^2 (Fig. 8 *B*), the principal changes of Z_T occur over a very small bandwidth (0.1 to 10 Hz) that is primarily in the frequency range of the Maxwell-Wagner dispersion. When R_p = 1 k$\Omega \cdot$ cm^2 (Fig. 8 *A*), the major changes of impedance occur over a range of frequencies (10 Hz–1 kHz) in the range of the α dispersion. At an intermediate R_p = 10 k$\Omega \cdot$ cm^2 (Fig. 8 *C*), the major changes of Z_T occur between 0.1 Hz and ~50 Hz, thereby encompassing the Maxwell-Wagner dispersion and a relatively small portion of the α dispersion. Thus, it should not be surprising, especially at these intermediate values of R_p, that the impedance loci cannot be described exactly by a simple equation of a single depressed semicircle.

For experimental data that appear to conform by inspection to an ideal (non-skewed) depressed semicircle, it is tempting to fit the data to a general and empirical equation of the form (Van Driessche, 1986):

$$Z_T = \frac{R^{fit}}{1 + (j\omega R^{fit} C^{fit}_{eq})^{\gamma^{fit}}} \quad (11)$$

Such an equation assumes that the impedance locus is symmetrical at frequencies above and below the frequency at the apex of the semicircle. The capacitance, C^{fit}_{eq}, is the capacitance at $\omega = (R^{fit}C^{fit}_{eq})^{-1}$. However, depending on the degree of asymmetry of the semicircle, the values of R^{fit} may be larger or smaller than those of R_T, depending on the

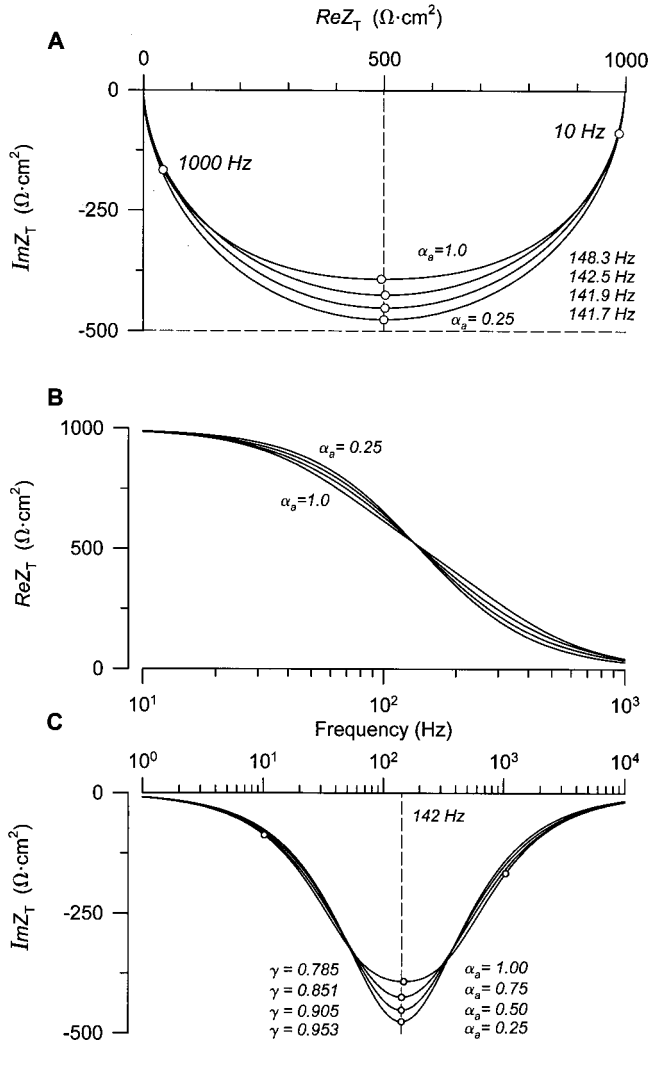

FIGURE 7 Influence of an apical membrane Cole-Cole dispersion on the transepithelial impedance (Z_T). R_p = 1000 Ω · cm², R_b = 4000 Ω · cm², C_b = 20.0 μF/cm², C_a^{dc} = 1.5 μF/cm², C_a^{∞} = 0.9 μF/cm², f^{τ} = 110 Hz. Calculations were done with α_a = 0.25, 0.5, 0.75, and 1.00. Corresponding values of depression of the impedance loci (γ) are indicated in (*C*).

range of Z_T included in fitting data to Eq. 11. Thus, for example, if the Z_T between 0.1 Hz and 50 Hz in Fig. 8 *C* are fit to Eq. 11, the fitted dashed line deviates from the actual data at frequencies >50 Hz (Fig. 8 *D*) and the value of C_{eq}^{fit} approximates the value of $|C_{eq}^{*}|$ at 12.09 Hz. Such fitting provides no information on the Maxwell-Wagner or α dispersions. Capacitance is calculated at a singular value of frequency at the apex of the fitted semicircle, where the frequency is determined not only by the capacitance, but also in particular by the value of R_p. Consequently, if R_p changes, then capacitance will appear to change due to the change of R_p and not due to change of the dielectric properties or area changes of the plasma membranes. For the conditions illustrated in Fig. 8 (R_p = 1, 10, and 50 kΩ · cm²), the values of C_{eq}^{fit} are remarkably close to the actual values of $|C_{eq}^{*}|$ at the frequencies, f^{z}.

It is also important to know that in the face of frequency-dependent capacitances there are experimental circumstances where impedance loci cannot be approximated by Eq. 11. For example, as illustrated in Fig. 9, we have calculated the impedance at values of R_p of 200, 600, and 1000 Ω · cm² assuming, ideally, that $R_a = \infty$ and that α_a = 1.0. Inspection of the plots in Fig. 9 *A* indicates clearly that it would be inappropriate to attempt to fit such data to Eq. 11, as the behavior of the impedance loci is certainly more complicated. This behavior, although influenced by the basolateral membrane R_b and C_b, is not due to a Maxwell-Wagner effect but rather to the apical membrane relaxation process as illustrated in Fig. 9 *B*, where the impedance loci were calculated with $R_b = 0$. Accordingly, the exaggerated asymmetry of the impedance loci in Fig. 9 *B* is due alone to the apical membrane dispersion that would be observed prevalently in "leaky" epithelia. If fitting of data at the higher frequencies is attempted with Eq. 11, the capacitances calculated would reflect those of the α dispersions at frequencies near 963 Hz when R_p = 200 Ω · cm².

If it is assumed that capacitance is constant at all frequencies, then it would be tempting to believe that data like those in Fig. 9 are best fit with a mathematical model consisting of an apical membrane R_aC_a and basolateral membrane R_bC_b that exist in parallel with R_p (see below). However, this would clearly be inappropriate here and would represent a serious pitfall when plasma membranes exhibit α dispersions. Thus, to avoid this pitfall, it would be prudent to evaluate epithelia for the existence of dispersions by any method appropriate to their transport physiology. For A6 epithelia and other tight epithelia where apical membranes express only Na^+ channels, the amiloride-blocked state of the tissues serves as such a method. Similarly, for very leaky tissues where $R_p \ll (R_a + R_b)$, frequency dependence due to Maxwell-Wagner or α dispersions can be assessed when the conditions of the experiments conform to Eq. 6.

Activation of apical membrane conductance

In response to second messengers like cAMP, the apical membrane conductances to Na^+ and Cl^- are activated in tissues like A6 epithelia resulting in decrease of R_a, and hence decrease of the fractional transcellular resistance $fR_a = R_a/(R_a + R_b)$. Depending on the relative values of R_a and R_b and their associated values of C_a^{*} and C_b^{*}, the transcellular impedance loci will, according to their time constants $R_aC_a^{*}$ and $R_bC_b^{*}$, reflect the existence of two plasma membranes in series by partially overlapping semicircles in Nyquist impedance plots dictated by the magnitudes of the impedance vectors of apical and basolateral membranes and the R_p of the paracellular shunt. Under absolutely ideal conditions when $R_p = \infty$ and C_a and C_b are constant at all frequencies, the transcellular impedance locus would appear as illustrated in

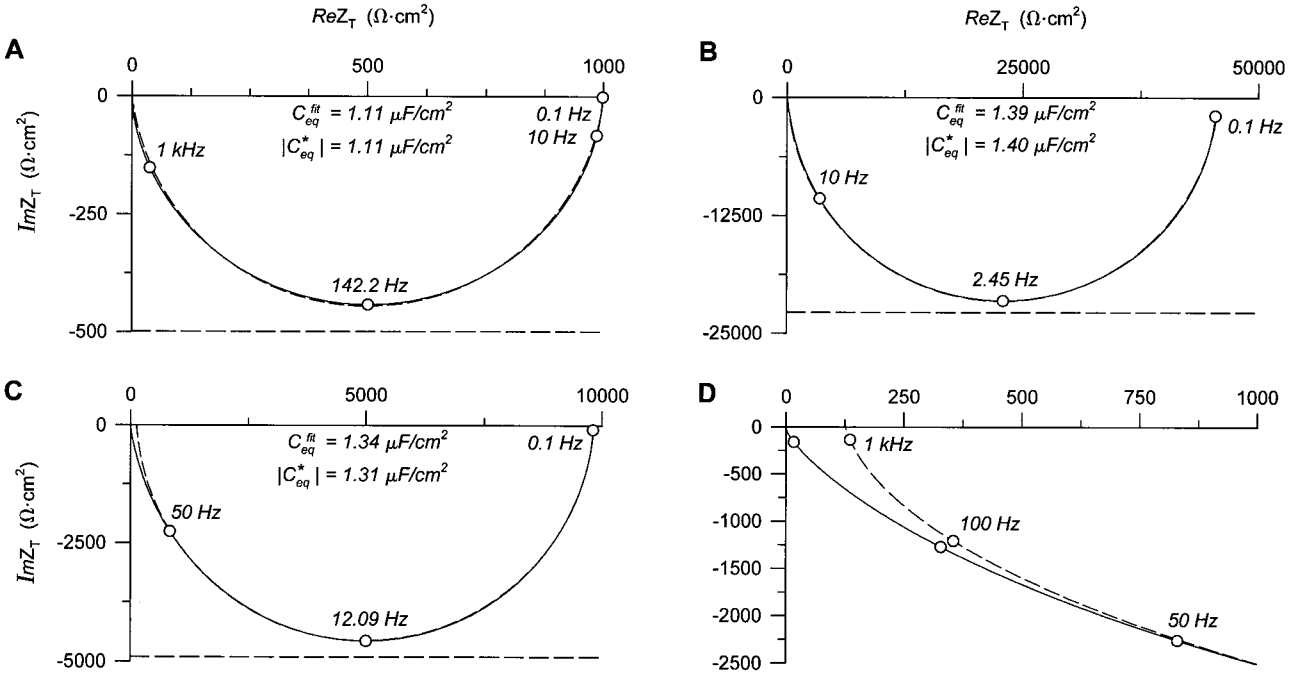

FIGURE 8 The solid lines are depressed Nyquist transepithelial impedance plots of tissues with shunt resistances, R_p, of 1000 $\Omega \cdot cm^2$ (*A*), 50,000 $\Omega \cdot cm^2$ (*B*), and 10,000 $\Omega \cdot cm^2$ (*C*). Other parameters are the same as in Fig. 5. Data were fitted with Eq. 11 to single depressed semicircles (*dashed lines*; see text). Frequency points are indicated by the open circles. Note that the impedance loci are depressed from the values expected (*horizontal dashed lines*) at the apices of the semicircles. Note also at the extremes of R_p in (*A*) and (*B*) that the fitted lines do not exactly superimpose Z_T over the entire range of frequency (see also Fig. 9). In (*C*) the fitted line deviates from Z_T at frequencies >50 Hz. This deviation is shown in expanded form in (*D*). The capacitances calculated at the apices of the fitted depressed semicircles, C_{eq}^{fit}, were 1.11 $\mu F/cm^2$ (142.2 Hz) (*A*); 1.34 $\mu F/cm^2$ (12.09 Hz) (*C*), and 1.39 $\mu F/cm^2$ (2.45 Hz) (*B*), respectively.

Fig. 10 *A*, where R_a and R_b are 1.5 and 4.0 $k\Omega \cdot cm^2$, respectively, and where C_a and C_b are 1.5 and 20 $\mu F/cm^2$, respectively. Although the time constants are sufficiently different at 2.0 Hz (R_bC_b) and 70.8 Hz (R_aC_a) to clearly indicate the existence of two membranes in series, ideal separation of the respective (non-depressed) semicircles would require a far greater difference in time constants to yield Nyquist plots that would clearly indicate the exact magnitudes of the R_a and R_b, and thus the series sum of the magnitudes of R_a and R_b on the real axis, ReZ_T. In practice, however, it would be most unusual for R_p to be infinitely large.

Plotted in Fig. 10 *B* are normalized impedance loci of the ideal cells (frequency-independent capacitance) shunted by R_p's of 50, 10, and 1 $k\Omega \cdot cm^2$ compared to the cells alone ($R_p = \infty$, Fig. 10 *A*). Such plots underscore the major influence played by R_p in determining the appearance of the impedance loci when R_p is in the range of values of R_a and R_b. Taken at face value, the plot with $R_p = 1\ k\Omega \cdot cm^2$ could be misinterpreted to indicate that $R_a > R_b$, when in fact this is not the case. Thus, it is critically important to obtain independent estimates of the R_p before fitting data to models to avoid the possibility of mischaracterizing the behavior of the cells in terms of their fractional transcellular resistances and capacitances.

To the extent that apical and basolateral membranes exhibit dielectric relaxations, analysis and fitting of data additionally require recognition that the impedance semicircles will be depressed (Awayda et al., 1999). Accordingly, for apical and basolateral membranes, respectively:

$$Z_a = \frac{R_a^{fit}}{1 + (j\omega R_a^{fit} C_a^{fit})^{\gamma_a^{fit}}} \quad (12)$$

$$Z_b = \frac{R_b^{fit}}{1 + (j\omega R_b^{fit} C_b^{fit})^{\gamma_b^{fit}}} \quad (13)$$

and $Z_T = ((Z_a + Z_b)R_p)/(Z_a + Z_b + R_p)$. Here, as above, formulation of such a model assumes that capacitance will be calculated at single frequencies corresponding to those at the time constants $R_a^{fit}C_a^{fit}$ and $R_b^{fit}C_b^{fit}$. To our knowledge there is no way to determine the frequency dependence of dielectric behavior at either the apical and/or basolateral membrane under these experimental conditions ($R_a \approx R_b$). Nevertheless, the existence of α dispersions would give rise to impedance loci that would require inclusion of power law dependencies (γ_a^{fit}, γ_b^{fit}) and hence, depressions of the impedance semicircles.

Illustrated in Fig. 11 are depressions of the impedance loci under conditions where C_a and/or C_b is complex (C_a^*, C_b^*). The data were calculated assuming that apical and/or basolateral membrane capacitances exhibit a single α dis-

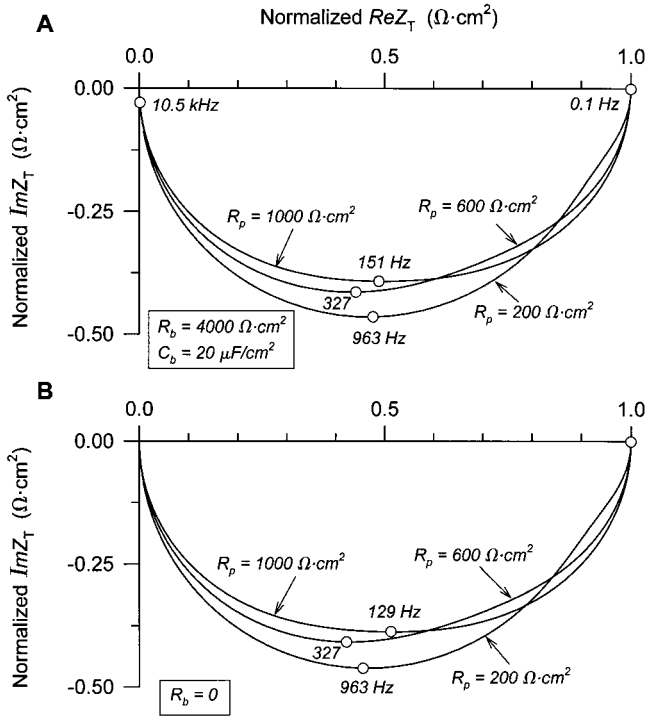

FIGURE 9 Shown are impedance loci normalized to values of R_p = 200, 600, and 1000 $\Omega \cdot cm^2$ that represent conditions where the impedance loci do not conform, even to a first approximation, to single depressed semicircles. In (*A*), R_b = 4000 $\Omega \cdot cm^2$ and C_b = 20 $\mu F/cm^2$. In (*B*) R_b = 0, indicating clearly that the asymmetric impedance loci shown in (*B*) originate from the apical membrane dielectric dispersion. $R_a = \infty$, C_a^{dc} = 1.5 $\mu F/cm^2$, C_a^{∞} = 0.9 $\mu F/cm^2$, f^{τ} = 110 Hz, α_a = 1.0. Impedance loci such as these cannot be fit to models (Eq. 11) that assume an equivalent cellular capacitance in parallel with an R_p.

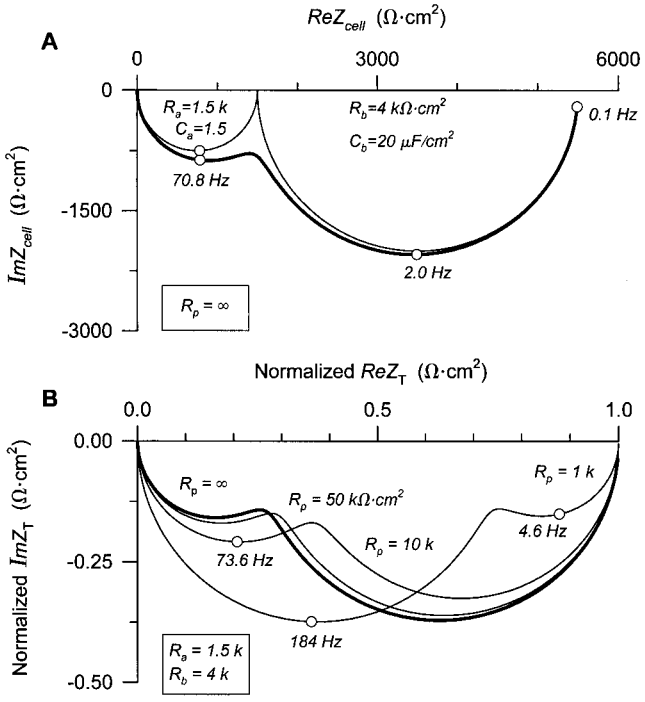

FIGURE 10 Activation of apical membrane conductance leads to interacting impedance semicircles in Nyquist plots. (*A*) Transcellular impedance (Z_{cell}) when R_a = 1500 $\Omega \cdot cm^2$ and R_b = 4000 $\Omega \cdot cm^2$. C_a (1.5 $\mu F/cm^2$) and C_b (20.0 $\mu F/cm^2$) were assumed to be independent of frequency. The magnitudes of the respective ideal (nondepressed) semicircles are shown by the thin solid lines that intersect the real axis so that $R_a + R_b = ReZ_T$ as frequency approaches zero. (*B*) Shown are transepithelial impedance loci normalized to their values of R_T when $R_p = \infty$, 50 k$\Omega \cdot cm^2$, and 1 k$\Omega \cdot cm^2$, indicating the dependence of the impedance locus on R_p when R_p is in the range of values of R_a and R_b.

persion at 110 Hz with a Cole-Cole power law coefficient α_a = 0.6. The assumed values of C_a^{dc} and C_b^{dc} are 1.5 and 20 $\mu F/cm^2$, and C_a^{∞} and C_b^{∞} are 0.9 and 12.0 $\mu F/cm^2$, respectively, when the capacitances are complex. When C_a^* alone is complex (Fig. 11 *A*), depression of the impedance locus is observed principally at higher frequencies corresponding to the frequency-dependent changes of capacitance associated with the apical membrane capacitance. Similarly, when C_b^* alone is complex (Fig. 11 *B*), depression of the impedance locus is observed principally at the lower frequencies corresponding to the frequency-dependent changes of capacitance associated with the basolateral membrane. When both C_a^* and C_b^* are complex (Fig. 11 *C*) the impedance locus is depressed over the entire range of frequency.

For the purpose of illustration we have specifically chosen a relaxation frequency of 110 Hz for the dispersions at both apical and basolateral membranes to show that the depressions of the impedance loci due to C_b^* would appear to be less than those for C_a^* even though $\alpha_a = \alpha_b = 0.6$ of the Cole-Cole dispersions. Because the impedance locus of the semicircle associated with C_b^* is centered over a relatively small band of frequencies near 2.7 Hz, the associated frequency-dependent changes of C_b^* are also relatively small. Consequently, there is no a priori reason to expect that γ_a^{fit} and γ_b^{fit} would be the same in value even though the dielectric properties of apical and basolateral membranes are the same. Thus, power law dependencies of the impedance loci bear no special relationships to the α dispersions, but as noted above give reason to believe that the capacitances are frequency-dependent.

Fitting of impedance data

We have noted above that estimating the cellular resistances and membrane capacitances can be troublesome when the R_p is finite and in the range of values of the R_a and R_b (see Fig. 10 *B*). For illustration, we have generated impedance data at identical frequencies used in our own experiments and used a least-squares nonlinear curve-fitting routine (Scientist, Micromath Scientific, Salt Lake City, UT) to fit the data over the parameter space of Eq. 1 where Z_a and Z_b are defined by Eqs. 12 and 13, respectively. R_a, R_b, and R_p were 1500, 4000, and 10,000 $\Omega \cdot cm^2$, respectively. We assumed

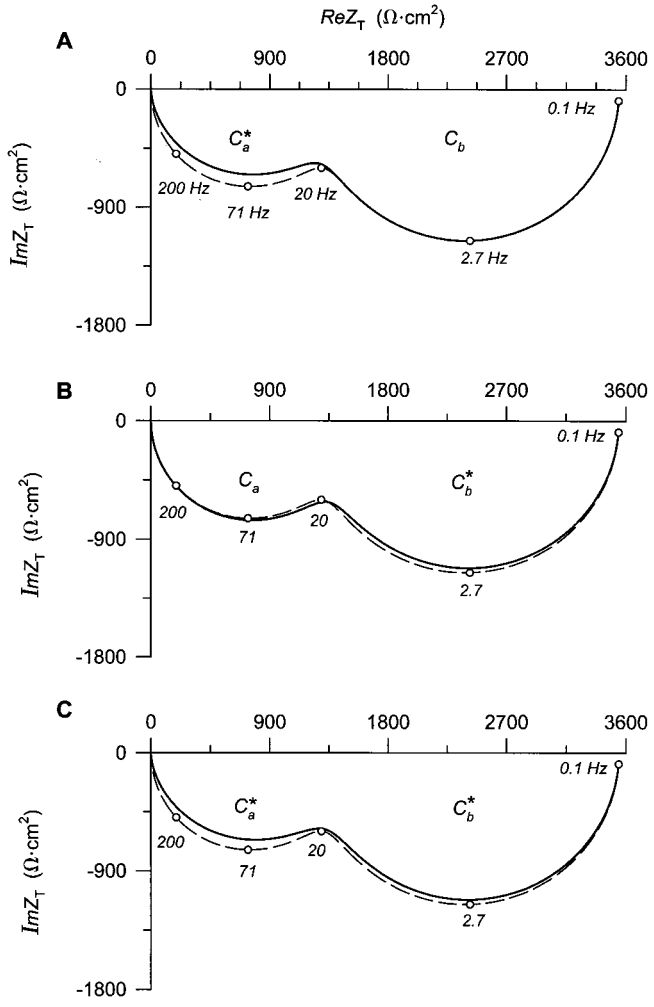

FIGURE 11 Solid lines show depressions of the transepithelial impedance locus when C_a is complex (C_a^*) (*A*), when C_b is complex (C_b^*) (*B*), and when both C_a and C_b are complex (*C*). Dashed lines show the impedance locus when C_a (1.5 μF/cm^2) and C_b (20.0 μF/cm^2) are independent of frequency. R_p = 10,000 $\Omega \cdot cm^2$, R_a = 1500 $\Omega \cdot cm^2$, R_b = 4000 $\Omega \cdot cm^2$. C_a^*: (C_a^{dc} = 1.5 μF/cm^2, C_a^{∞} = 0.9 μF/cm^2, f^{τ} = 110 Hz, α_a = 0.6). C_b^*: (C_b^{dc} = 20.0 μF/cm^2, C_b^{∞} = 12.0 μF/cm^2, f^{τ} = 110 Hz, α_b = 0.6).

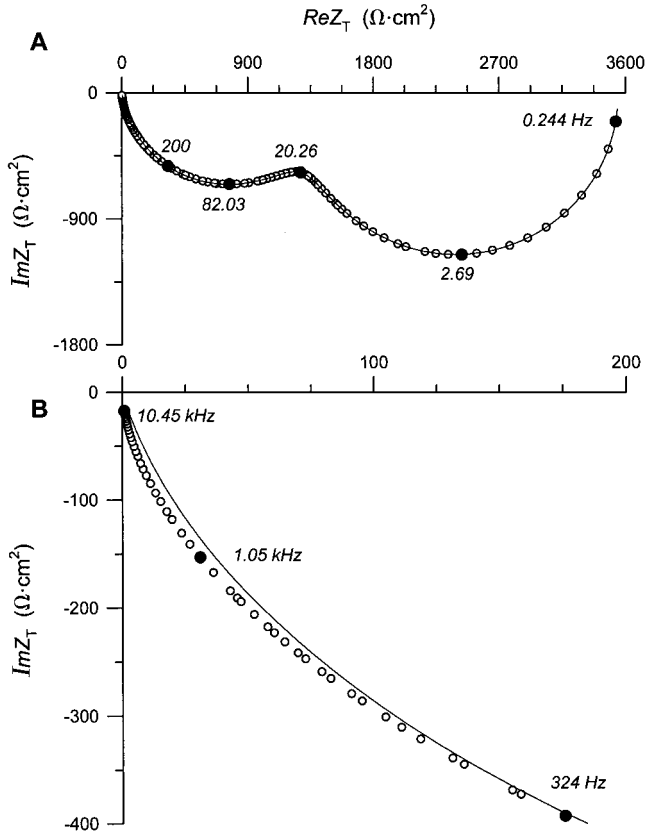

FIGURE 12 Transepithelial impedance data (0.244–200 Hz) were subjected to nonlinear curve-fitting to a model of apical and basolateral membrane depressed semicircles (see text) (*A*). R_p = 10,000 $\Omega \cdot cm^2$, R_a = 1500 $\Omega \cdot cm^2$, R_b = 4000 $\Omega \cdot cm^2$. C_a^*: (C_a^{dc} = 1.5 μF/cm^2, C_a^{∞} = 0.9 μF/cm^2, f^{τ} = 110 Hz, α_a = 0.6). C_b = 20.0 μF/cm^2. Note deviation of fitted line from the actual data points at frequencies >324 Hz (*B*).

a frequency-independent C_b = 20.0 μF/cm^2 and an apical membrane C_a^* with an α dispersion centered at 110 Hz like the one described above. The Nyquist plot of the data points and the fitted line are shown in Fig. 12. Although the fitted line is not perfect at frequencies above ~324 Hz (Fig. 12 *B*), the errors in estimation of the R_a (R_a^{fit} = 1528 $\Omega \cdot cm^2$), R_b (R_b^{fit} = 4014 $\Omega \cdot cm^2$), and R_p (R_p^{fit} = 9857 $\Omega \cdot cm^2$) are <~1.5%. As expected, the γ_a^{fit} was depressed (0.915) while the γ_b^{fit} was not depressed (1.00). C_b^{fit} at 1.97 Hz was 20.11 μF/cm^2. C_a^{fit} at 83.9 Hz was 1.24 μF/cm^2 and was identical in value to the $|C_a^*|$ of the α dispersion at this frequency.

If we assumed additionally that both C_a^* and C_b^* were complex, and the data so generated (not shown) were fit as above, the errors in estimation of the R_a (R_a^{fit} = 1568 $\Omega \cdot cm^2$), R_b (R_b^{fit} = 4012 $\Omega \cdot cm^2$), and R_p (R_p^{fit} = 9795 $\Omega \cdot cm^2$) were <~4.5%. γ_a^{fit} was depressed (0.912) and the γ_b^{fit} was also depressed (0.987). C_b^{fit} at 1.98 Hz was 20.0 μF/cm^2 compared to the $|C_b^*|$ of 19.59 μF/cm^2. C_a^{fit} at 82.9 Hz was 1.23 μF/cm^2 and was identical in value to the $|C_a^*|$ of the α dispersion at this frequency. Thus, to a good approximation, and despite frequency dependence of capacitance, the R_a, R_b, and R_p can be determined with reasonable certainty. However, the capacitances are constrained to those at specific frequencies dictated not only by the R_a and R_b, but also the R_p. Accordingly, in the face of changes of R_a, R_b, and/or R_p, changes of C_a^{fit} and/or C_b^{fit} cannot be attributed only to changes of membrane area when membranes exhibit dielectric dispersions. Indeed, because changes of capacitance can occur in the absence of change of membrane area through change of relaxation frequencies and/or dielectric increments at any frequency (Awayda et al., 1999), independent methods are required to assure that changes of capacitance reflect change of membrane area.

We gratefully acknowledge the assistance of A. L. Helman and her help in preparation of this manuscript. This work was supported by National

Institute of Diabetes and Digestive and Kidney Diseases Grant DK30824, the University of Illinois at Urbana-Champaign Campus Research Board, and postdoctoral fellowship support to T.G.P. from the National Kidney Foundation and its Illinois Affiliate.

REFERENCES

Awayda, M. S., W. Van Driessche, and S. I. Helman. 1999. Frequency-dependent capacitance of the apical membrane of frog skin: dielectric relaxation processes. *Biophys. J.* 76:219–232.

Baxendale-Cox, L. M., R. L. Duncan, X. Liu, K. Baldwin, W. J. Els, and S. I. Helman. 1997. Steroid hormone-dependent expression of blocker-sensitive ENaCs in apical membranes of A6 epithelia. *Am. J. Physiol. Cell Physiol.* 273:C1650–C1656.

Blazer-Yost, B., X. Liu, and S. I. Helman. 1996. Insulin stimulated Na^+ transport is mediated by increase of apical Na^+ channels and not open probability in control and aldosterone pre-stimulated A6 epithelia. *FASEB J.* 10:78*a* (Abstr.).

Blazer-Yost, B. L., T. G. Păunescu, S. I. Helman, K. D. Lee, and C. J. Vlahos. 1999. Phosphatidylinositol 3-kinase is required for aldosterone regulated sodium reabsorption. *Am. J. Physiol. Cell Physiol.* 277: C531–C536.

Chalfant, M. L., B. Coupaye-Gerard, and T. R. Kleyman. 1993. Distinct regulation of Na^+ reabsorption and Cl^- secretion by arginine vasopressin in the amphibian cell line A6. *Am. J. Physiol. Cell Physiol.* 264: C1480–C1488.

Chua, L. O. 1969. Introduction to Nonlinear Network Theory. McGraw Hill, Inc., New York.

Cole, K. S. 1968. Membranes, Ions and Impulses. University of California Press, Berkeley.

Cole, K. S., and R. H. Cole. 1941. Dispersion and absorption in dielectrics. I. Alternating current characteristics. *J. Chem. Phys.* 9:341–351.

Daniel, V. V. 1967. Dielectric Relaxation. Academic Press, London.

Gabler, R. 1978. Electrical Interactions in Molecular Biophysics. Academic Press, New York.

Goldman, D. E. 1943. Potential, impedance, and rectification in membranes. *J. Gen. Physiol.* 27:37–60.

Gordon, L. G. M., G. Kottra, and E. Fromter. 1989. Electrical impedance analysis of leaky epithelia: theory, techniques, and leak artifact problems. *In* Methods in Enzymology, Vol. 171. Biomembranes Pt. R, Transport Theory: Cells and Model Membranes. S. Fleischer and B. Fleischer, editors. Academic Press, San Diego. 643–663.

Helman, S. I., and X. Liu. 1997. Substrate-dependent expression of Na^+ transport and shunt conductance in A6 epithelia. *Am. J. Physiol. Cell Physiol.* 273:C434–C441.

Helman, S. I., X. Liu, K. Baldwin, B. L. Blazer-Yost, and W. J. Els. 1998. Time-dependent stimulation by aldosterone of blocker-sensitive ENaCs in A6 epithelia. *Am. J. Physiol. Cell Physiol.* 274:C947–C957.

Helman, S. I., and S. M. Thompson. 1982. Interpretation and use of electrical equivalent circuits in studies of epithelial tissues. *Am. J. Physiol. Renal Physiol.* 243:F519–F531.

Jonscher, A. K. 1983. Dielectric Relaxation in Solids. Chelsea Dielectrics Press, London.

Kell, D. B., and C. M. Harris. 1985. On the dielectrically observable consequences of the diffusional motions of lipids and proteins in membranes. 1. Theory and overview. *Eur. Biophys. J.* 12:181–197.

Kokko, K. E., P. S. Matsumoto, Z. R. Zhang, B. N. Ling, and D. C. Eaton. 1997. Prostaglandin E_2 increases 7-pS Cl^- channel density in the apical membrane of A6 distal nephron cells. *Am. J. Physiol. Cell Physiol.* 273:C548–C557.

Liu, X., and S. I. Helman. 1998. Time-dependent increases of apical membrane capacitance of A6 epithelia caused by aldosterone. *FASEB J.* 12:123*a*. (Abstr.).

Marunaka, Y., and D. C. Eaton. 1990. Chloride channels in the apical membrane of a distal nephron A6 cell line. *Am. J. Physiol. Cell Physiol.* 258:C352–C368.

Matsumoto, P. S., L. Mo, and N. K. Wills. 1997. Osmotic regulation of Na^+ transport across A6 epithelium: interactions with prostaglandin E_2 and cyclic AMP. *J. Membr. Biol.* 160:27–38.

Nakahari, T., and Y. Marunaka. 1995. ADH-evoked $[Cl^-]_i$-dependent transient in whole cell current of distal nephron cell line A6. *Am. J. Physiol. Renal Physiol.* 268:F64–F72.

Păunescu, T. G., B. L. Blazer-Yost, C. J. Vlahos, and S. I. Helman. 2000. LY-294002-inhibitable PI 3-kinase and regulation of baseline rates of Na^+ transport in A6 epithelia. *Am. J. Physiol. Cell Physiol.* 279: C236–C247.

Păunescu, T. G., and S. I. Helman. 2001. PGE_2 activation of apical membrane Cl^- channels in A6 epithelia: impedance analysis. *Biophys. J.* 81:852–866.

Pethig, R. 1979. Dielectric and Electronic Properties of Biological Materials. John Wiley & Sons, New York.

Schifferdecker, E., and E. Fromter. 1978. The AC impedance of Necturus gallbladder epithelium. *Pflugers Arch.* 377:125–133.

Schwan, H. P. 1957. Electrical properties of tissue and cell suspensions. *In* Advances in Biological and Medical Physics, Vol. V. J. H. Lawrence and C. A. Tobias, editors. Academic Press, New York. 147–209.

Takashima, S. 1989. Electrical Properties of Biopolymers and Membranes. Adam Hilger, Bristol.

Van Driessche, W. 1986. Lidocaine blockage of basolateral potassium channels in the amphibian urinary bladder. *J. Physiol.* 381:575–593.

Yanase, M., and J. S. Handler. 1986. Adenosine 3′,5′-cyclic monophosphate stimulates chloride secretion in A6 epithelia. *Am. J. Physiol. Cell Physiol.* 251:C810–C814.